In situ thermochemical sulfate reduction during ore formation at the Itxaspe Zn-(Pb) MVT occurrence (Basque-Cantabrian basin, Northern Spain)

A. Pique, Angels Canals, Jean-Robert Disnar, F. Grandia

In situ thermochemical sulfate reduction during ore formation at the Itxaspe Zn-(Pb) MVT occurrence (Basque-Cantabrian basin, N Spain)

À. Piqué[(1)] À. Canals[(1)] J.R. Disnar[(2)] F. Grandia[(3)]

(1) Departament de Cristal·lografia, Mineralogia i Dipòsits Minerals, Facultat de Geologia, Universitat de Barcelona, C. Martí i Franquès s/n, 08028 Barcelona, Spain. angelspique@ub.edu, fax. +34934021340

(2) Institut des Sciences de la Terre d'Orléans, UMR 6113 du CNRS et de l'Université d'Orléans, 1A Rue de la Férollerie, 45071 Orléans Cédex 2, France.

(3) Amphos XXI Consulting S.L., Pg. de Rubí 29-31, 08197 Valldoreix, Spain.

ABSTRACT

Organic matter is thought to play a role in the genesis of many Mississippi Valley-type (MVT) deposits, acting as a reducing agent during thermochemical sulfate reduction (TSR). Although TSR is an extremely slow reaction at low temperatures (<100ºC), under favorable conditions it may possibly supply the necessary reduced sulfur during ore formation. To test this hypothesis, the Itxaspe Zn-(Pb) MVT occurrence in the Basque-Cantabrian basin (N Spain), was studied. Sphalerite, the main ore phase, is generally found disseminated in Urgonian (Lower Cretaceous) carbonates, and in close relationship with solid bitumen. The bitumen source rock was very likely deposited in a marine marginal setting. Differences in composition of the bitumen samples are attributed to a fractionation during hydrocarbon expulsion and/or migration. The fluids involved in ore deposition were low temperature (T_h ~130ºC), Na-Ca-Cl-(K-

Mg)-type brines (salinities ~12.5 equiv. mass % NaCl). The origin of brine solutes (including sulfate) is related to the dissolution of Mesozoic evaporite units, although the contribution of evaporated seawater brines cannot be ruled out. The temperatures of ore deposition, the close relationship between the bitumen and ore phases, the presence of aromatic sulfur-bearing compounds and the $\delta^{34}S$ of sulfides and sulfates are consistent with an in situ TSR during ore formation in the Itxaspe Zn-(Pb) occurrence. Therefore, at least for small mineralizations like Itxaspe, our conclusion is that the necessary reduced sulfur can be supplied by TSR during ore genesis at the site of metal deposition.

KEYWORDS: Bitumen. Thermochemical sulfate reduction. Mississippi Valley-type deposits. Basque-Cantabrian basin.

INTRODUCTION

The association of organic matter with Zn-Pb Mississippi Valley-type (MVT) deposits is common worldwide (e.g., Powell and Macqueen, 1984; Leventhal, 1990; Kesler et al., 1994; Disnar, 1996; Hu et al., 1998; Spangenberg and Macko, 1998; Selby et al., 2005; among others). Under certain conditions, this organic matter can be directly involved in the reduction of aqueous sulfate, leading subsequently to base metal sulfide deposition (e.g., Powell and Macqueen, 1984; Leventhal, 1990). Organic matter-mediated sulfate reduction can occur either by bacterial activity (bacterial sulfate reduction; BSR) or by an abiological reaction called thermochemical sulfate reduction (TSR), in two mutually exclusive thermal regimes (e.g., Machel, 2001). In contrast to BSR, TSR is known to be an extremely slow process, although, under favorable

circumstances it can be fast enough to generate H_2S during ore formation in MVT deposits (e.g., Thom and Anderson, 2008).

The present work deals with the Itxaspe Zn-(Pb) occurrence, an example of MVT mineralization closely associated with organic matter, where the reduced sulfur is proposed to be a product of in situ TSR during ore formation. This mineralization is located in the Mesozoic Basque-Cantabrian basin (BCB) in northern Spain (Fig. 1), and consists of small (50 x 50 to 200 x 200 m) ore bodies of disseminated sphalerite, together with minor galena and bournonite (IGME-EVE, 2000). The aim of the present study is to elucidate the origin and the role of organic matter in the genesis of the ore, which in turn can help in the improvement of genetic models for this type of mineralization; all by means of detailed paragenetic and textural studies, and organic matter (reflectivity, Rock-Eval, GC-MS and on-line py-GC-MS) fluid inclusion (microthermometry and crush-leach) and stable isotope (S, C and O of ore and gangue phases) characterization.

The Itxaspe Zn-(Pb) occurrence belongs to an important district of hydrothermal Zn-Pb and Fe deposits in the BCB (Fig. 1). Most of these mineralizations are MVTs (e.g., Barbanson, 1987; Herrero, 1989; Gil, 1991; Velasco et al., 1994; Perona et al., 2007), including the world-class deposit of Reocín (62 Mt of ore @ 8.7% Zn and 1% Pb; Velasco et al., 2003), although a few of them were considered to be of Sedex type (e.g. Troya; Fernández-Martínez and Velasco, 1996). They are mainly stratabound or vein type and the stratabound are generally constrained to three Urgonian (Lower Cretaceous) carbonate units (Velasco et al., 1994). In some of the MVT deposits, organic matter has been found in close relationship with the ore phases (e.g., Barbanson, 1987; Perona et al., 2004) and this organic matter may have played a significant role

during transport and/or deposition of the base metals (Hu et al., 1998). The BCB is also attractive for hydrocarbon exploration: oil and gas production have been established both onshore (Ayoluengo oil field and Castillo gas field) and offshore (Gaviota and Albatros gas fields) (Fig. 1), and several non-commercial oil discoveries have also been reported (Quesada et al., 1997).

GEOLOGIC SETTING

The BCB is a Mesozoic extensional basin in northern Spain, surrounded by several massifs of Paleozoic materials (Fig.1). The basin is mainly filled with sediments of Cretaceous age, with thicknesses that can reach more than 15 km (e.g., García-Mondéjar, 1989). Its evolution is linked to extensional processes related to the opening of the North Atlantic Ocean and the Bay of Biscay.

A first event of rifting took place during the Lower Triassic, resulting in the development of an intra-cratonic basin and the deposition of Buntsandstein, Muschelkalk and Keuper facies sediments. The Lower and Middle Jurassic materials correspond to platform carbonates and marls (Rat, 1987). A new rifting event began during the Upper Jurassic, changing the former structures and building up a new basin. From the Kimmeridgian to Barremian the sedimentation was clastic (Rat, 1987). Later on, the Urgonian Complex was deposited in Aptian and Albian times, and the basin was subdivided by NW-SE strike-slip faults into several pull-apart basins (García-Mondéjar, 1989; García-Mondéjar et al., 1996). These faults have been related to strike-slip movements of the Iberian and European plates during the opening of the Bay of Biscay. In those times Itxaspe was part of the Lekeitio uplift, limited by the strike-slip faults and subdivided by NE-SW synsedimentary faults (García-Mondéjar et al., 1996).

In the BCB, the Urgonian Complex hosts most of the Zn-Pb and Fe mineralizations. It consists of four cyclic depositional sequences related to tectonic pulses and relative sea-level changes, characterized by the alternation of terrigenous sediments and platform carbonates and by the presence of unconformities (see e.g., García-Mondéjar, 1990 for further details). The Urgonian sediments were covered by the Supra-Urgonian Complex, which consists of siliciclastic materials deposited in continental, deltaic and slope environments. In the northern part of the basin the sedimentation was mainly of flysch type. Several outcrops of Albian to Santonian alkaline submarine lavas occur related to the rift and/or transform faults (Carracedo et al., 1999). Upper Cretaceous-Paleocene materials mainly correspond to continental detrital sediments, platform carbonates and flysch marls (Rat, 1987). During the Tertiary, the Alpine compression produced a tectonic inversion of the BCB (Gómez et al., 2002).

Geology and metallogeny of Itxaspe

Itxaspe is located in the northern Biscay anticlinorium, developed during the Alpine orogeny (Gómez et al., 2002; Fig. 1). The area is constituted by Urgonian Complex rocks, including from bottom to top: calcareous siltstones, marls, marly limestones and limestones, changing laterally and upwards to reefal limestones and ending with marls, calcarenites and lutites (Fig. 2). Supra-Urgonian flysch corresponds to an alternation of lutites and sandstones, and Cenomanian to Santonian calcareous flysch to an alternation of marls and marly limestones (Fig. 2).

The study area is affected by a network of faults and Alpine thrusts, together with folds in the flysch materials (Fig. 2). The alpine compression reinforced the

Mesozoic subdivision in horsts and grabens of the Urgonian limestones, which show an intense fracturing (IGME-EVE, 2000).

In an abandoned mining area around the village of Itxaspe, up to nine Zn-Pb occurrences were discovered in late 1980s during a drilling program by Outokumpu and Ente Vasco de la Energía (EVE). The Zn-Pb occurrences are stratabound, generally located at the top of the Urgonian reefal carbonates and close to main faults. Also breccias and marls were found to be mineralized. The ore bodies have sizes between 50 x 50 to 200 x 200 m and up to 20 m thick of disseminated ore. The paragenesis is rather simple, with sphalerite as the most abundant sulfide, together with galena, bournonite, pyrite, marcasite, barite and calcite as accessory phases. A silicification of the host rock is usually found together with the mineralization and occasionally, geodes filled with calcite, marcasite and solid bitumen are found in the host limestones (IGME-EVE, 2000).

METHODOLOGY

Samples for the study were collected from four boreholes (ITX13, ITX16, ITX20 and ITX28), drilled by Outokumpu and EVE (see location on Fig. 2). All the observations, measurements and analyses were done at the Universitat de Barcelona, unless otherwise noted. Mineralogical and textural studies were carried out on hand specimens and under white (transmitted and reflected) light and cathodoluminescence (CL) microscopy.

Fluid inclusion microthermometry was conducted on double-polished sphalerite samples, using a Linkam THMSG-600 heating-freezing stage. The stage was calibrated with inclusions of pure CO_2 and of distilled water. The precision was ± 0.1ºC below 0ºC

and ± 2ºC for homogenization temperatures. Salinity of fluid inclusions, reported in equiv. mass % NaCl, was calculated with the computer program BULK (Bakker, 2003) and the equation of Bodnar (1993). Crush-leach analysis of fluid inclusions was carried out at the School of Earth and Environment, University of Leeds, and the analytical procedure is described in detail in Banks et al. (2000). Anions (Cl^- and Br^-) were determined with a Dionex DX-500 ion chromatograph and cations (Li^+, Na^+ and K^+) with a Varian flame emission spectrometer. The analytical precision was better than 10% (2σ).

The sulfur and oxygen isotope composition of barite, sulfur isotope composition of sulfides, as well as carbon and oxygen isotope composition of carbonates were determined. Prior to isotope analysis, carbonate samples were cleaned with NaOCl to remove the soluble organic matter, following the procedure of Charef and Sheppard (1984). The $\delta^{34}S$ was determined with a Carlo Erba 1108 elemental analyzer and the $\delta^{18}O_{SO4}$ with a TC-EA, both coupled to an IRMS Thermo Finnigan Delta Plus XP. The $\delta^{18}O$ and $\delta^{13}C$ of carbonates were analyzed with an IRMS Finnigan MAT 252 coupled to a Carbonate Kiel Device. Isotope ratios, expressed in δ per mil relative to the VCDT for sulfur, VSMOW for oxygen and VPDB for carbon, were calculated using international and internal laboratory standards with reproducibilities of ±0.2‰ for $\delta^{34}S$ and $\delta^{18}O_{SO4}$, ±0.02‰ for $\delta^{13}C$ and ±0.05‰ for $\delta^{18}O_{CO3}$.

The study of organic matter was carried out at the Institut des Sciences de la Terre d'Orléans (ISTO). Microscopic observations were performed with a Leica DMR XP microscope under white (reflected and transmitted) and ultraviolet light. Random reflectivity measurements (expressed in %) were made on polished samples, following the procedures of the International Committee for Coal Petrology (1971) and using an

oil immersion objective (x50). Rock-Eval analyses were carried out with a "Turbo" model RE6 pyrolyzer (Vinci Technologies), in standard conditions. The basic operating principles of the Rock-Eval apparatus are described in Lafargue et al. (1998). Five samples were analyzed for their free hydrocarbon content by gas chromatography-mass spectrometry (GC-MS). On three out of these five samples (the poorest in TOC) the free hydrocarbons were analyzed after extraction with dichloromethane (with activated copper foil to ensure desulfurization) and evaporation of the solvent without any fractionation. For the two other samples, the bitumen extracted with CH_2Cl_2 was first de-asphalted with n-heptane, then fractioned into saturates, aromatics and resins on a Florisil® (60-100 mesh) mini-column by successive elution with n-heptane, with a mixture of n-heptane and toluene (2:1 volume ratio) and finally with methanol. All analyses were performed with a Thermo Finnigan TRACE GC–MS, equipped with an Rtx®-5Sil MS capillary column (30 m x 0.32 mm i.d., 0.25 μm film thickness) with 5 m of guard column. The GC operating conditions were as follows: temperature hold at 40°C for 1 min, then increase from 40 to 120°C at 30°C/min, 120 to 300°C at 3°C/min with final isothermal hold at 300°C for 30 min. The samples were injected splitless, with the injector temperature set at 280°C. Helium was the carrier gas. The mass spectrometer was operated in the electron ionization mode at 70 eV of ionization energy and scanned from 50 to 650 Daltons. Organic compounds were identified by comparison with library (NIST) mass spectra and relative retention times. On-line pyrolyses (py–GC–MS) were performed with a Curie point Fischer GSG flash pyrolyzer directly coupled to the GC–MS. Samples were pyrolyzed for 10 s under helium flow, using a ferromagnetic wire with a Curie temperature of 670°C. The analyses were carried out under the same conditions quoted above except for the temperature program

that was the following one: 50°C (hold 5 min), raise from 50 to 300°C at 4°C/min and final isothermal hold at 300°C for 10 min.

PARAGENESIS AND TEXTURES OF THE MINERALIZATION

In the studied drill cores the mineralization is hosted in Urgonian mudstones, wackestones and breccias (Fig. 2 and Fig. 3), the latter consisting of cm-sized carbonate and/or aluminosilicate fragments in a lutitic matrix. In the four studied boreholes, breccias are always found mineralized (Fig. 2). Regardless of the host rock lithology, ore phases are generally disseminated (Fig. 2 and Fig. 3A, B) and only locally are massive (Fig. 3C) or in veinlets (Fig. 3D). Disseminated ore can be found continuously in more than 20 m of drill core. In contrast, massive ore bands are less than 0.5 m thick (Fig. 2). The cm- to mm-thick veinlets are filled with ore and gangue minerals (Fig. 3D) and represent the volumetrically less important style of mineralization. The host rocks are usually silicified (Fig. 2), especially the breccias, where microcrystalline quartz, together with the ore phases occur mainly in the matrix (Fig. 3A, D) and in the carbonate fragments.

The paragenesis, deduced from the observations of hand samples and 29 thin sections, consists of sphalerite as the main ore mineral, together with galena, bournonite and minor amounts of tetrahedrite, chalcopyrite, pyrite and marcasite. Other coexisting phases include quartz, barite, calcite and solid bitumen. The paragenetic sequence has been subdivided into three stages: (1) pre-ore stage; (2) ore stage; and (3) post-ore stage(s) (Fig. 4). The pre-ore stage corresponds to the beginning of the host rock silicification, characterized by the precipitation of quartz, together with minor μm-sized pyrite, marcasite and phyllosilicates.

During the ore stage, quartz, sphalerite, galena, bournonite and minor tetrahedrite, chalcopyrite, pyrite and marcasite precipitated. These phases replaced the host rock and at the end of the stage also precipitated in veinlets. Two sphalerite generations have been distinguished: an early and most abundant brown-colored sphalerite, zoned, euhedral to subhedral (Fig. 5A) and relatively coarse (up to 5 mm in size); and a late, honey-colored sphalerite occurring as overgrowths on the early sphalerite and also in veinlets (Fig. 5B). The other sulfides and sulfosalts are euhedral to anhedral and fine-grained (<1 mm-sized). Quartz from this stage is euhedral, can reach up to 2 mm and has inclusions of bitumen in growth bands (Fig. 5C). Patches of solid bitumen are found in close association with the sulfides (Fig. 5D), in veins and cavities and also filling fossil moulds in limestones. Some of this solid bitumen show degassing bubbles and contraction cracks (Fig. 5D).

Barite and calcite precipitated at the end of the ore stage, both in veins, together with quartz and sulfides, and replacing the host rock. Calcite crystals are generally <4 mm, while barite is μm-sized and forms fan-shaped aggregates (Fig. 5E). During the post-ore stage, calcite and barite continued to precipitate in veinlets and filling bitumen and sulfide cracks. Late quartz partially or completely replaced the host rock and early barite, calcite, sulfides and sulfosalts. At least for the case of sphalerite, the replacement was isovolumetric (Fig. 5F). Quartz and calcite veinlets are found crosscutting all previous assemblages and structures.

FLUID GEOCHEMISTRY

Fluid inclusion study

A total of 57 fluid inclusions were characterized and measured in a sample of massive sphalerite (ITX13-3) and three more were measured in sphalerite disseminated in limestone (ITX16-4). The low degree of transparency of sphalerite precluded the fluid inclusion study in the other samples. The fluid inclusions are generally smaller than 30 μm and have elongated, irregular or negative crystal shapes. Most of them are found in clusters and some appear isolated. They are two-phase (liquid + vapor) at room temperature and the vapor bubble occupies less than 5% of total inclusion area.

First observed melting temperatures (between –53 and –46ºC) were close to the eutectic temperatures (T_e) of the H_2O-NaCl-$CaCl_2$ (T_e= –52ºC) and H_2O-NaCl-$CaCl_2$-$MgCl_2$ (T_e= –57ºC) systems (Davis et al., 1990). Ice was the last solid to melt, at temperatures between –13.4 and –5.7ºC (n = 55), with a mode at -8.7ºC (Fig. 6A), corresponding to a salinity of 12.5 equiv. mass % NaCl. Hydrohalite melting temperatures (T_{mhy}) were between –23.6 and –22.7ºC (n = 3), equivalent to Ca/Na ratios between 0.25 and 0.4 by weight in the NaCl-$CaCl_2$-H_2O diagram from Oakes et al. (1990). Homogenization was to the liquid phase, at temperatures (T_h) between 80 and 152ºC (n = 50), with a mode at 130ºC (Fig. 6B).

Crush-leach analyses of inclusion fluids were done in the same sphalerite samples studied by microthermometry and in late stage calcite from sample ITX16-4 (Table 1). In order to calculate the Ca/Na ratios, a charge balance of crush-leach data was done assuming Cl^-, Na^+, K^+ and Ca^{2+} as the major ions in solution. For calcite fluids, the calculated Ca/Na ratio is 0.5 by weight, which is quite similar to those obtained from T_{mhy} of brines trapped in sphalerite. In contrast, the crush-leach analyses done in sphalerite have a deficit of anions.

Cl^- and Br^- are generally considered as conservative tracers, unless evaporite dissolution or precipitation takes place. Therefore, Cl/Br ratios have been extensively used to discriminate between different fluids and to provide information on the origin of their salinity (e.g., Grandia et al., 2003 and references therein). Cl/Br ratios in the analyzed brines (Table 1) are much higher than present-day seawater (molar ratio of 658; Fontes and Matray, 1993), elucidating the contribution of halite-dissolution fluids to the salinity. The values are also consistent with the involvement of seawater or brines with some degree of evaporation, as pointed Grandia et al. (2003) to explain similar data from peridiapiric Zn-Pb ores in the BCB. According to the results, the bulk of fluids trapped in sphalerite from Itxaspe have a higher contribution of halite-dissolution brines than those trapped in late stage calcite.

The ratios involving cations such as Na, K and Li are more sensitive to water-rock interaction processes. This is evidenced in the Itxaspe data, which have lower Na/Br and much lower Na/K and Na/Li ratios than those expected from the mixing of halite-dissolution brines with seawater or more evolved brines (see Grandia et al., 2003 for further details). Therefore, other mechanisms such as interactions with siliciclastic rocks should be considered.

Stable isotopes

The sulfur isotope composition was determined on eleven sphalerite, four barite and one galena samples (Table 2). $\delta^{34}S$ of sphalerite are between +3.5 and +17.7‰, galena has the lowest $\delta^{34}S$ (+3.3‰) and $\delta^{34}S$ of barite range from +18.3 to +23.1‰. $\delta^{18}O$ of the same barite are between +15.6 and +17.8‰. Following the constraints provided by the halogen data, a plausible sulfur source could be sulfate leached from the

Triassic-Liasic evaporites, but also sulfate from seawater or from evolved basinal brines. The $\delta^{34}S$ of Keuper gypsum from the BCB is close to +15‰ (Boyce et al., 1990; Perona et al., 2007), while the $\delta^{34}S$ of Mesozoic marine evaporites fluctuated between +13 and +20‰ and the $\delta^{18}O$ between +10 and +15‰ (Claypool et al., 1980).

The $\delta^{13}C$ and $\delta^{18}O$ was determined on 16 samples of carbonates: five corresponding to ore stage calcites, six to post-ore stage calcites and other five to host limestones (Table 2). The Lower Cretaceous marine limestones from the BCB have isotope compositions constrained to +27.2±1.7‰ for oxygen and +2.8±1.1‰ for carbon (Velasco et al., 1994; Bustillo and Ordoñez, 1995; Simón et al., 1999; Velasco et al., 2003). The $\delta^{13}C$ of the host limestones (between +2.4 and +3.5‰) are within the range of the regional values, whereas the $\delta^{18}O$ (between +21.2 and +26.9‰) show a higher variability, with most samples depleted in ^{18}O (Table 2). Since $\delta^{18}O$ is sensitive to temperature changes, this depletion could indicate an interaction with a hot fluid, but also with isotopically lighter waters.

Ore stage calcites are more depleted in ^{18}O than the host limestones, with values between +17.8 and +20.4‰, while $\delta^{13}C$ are between –1.7 and +3.6‰. Post-ore stage calcites have intermediate $\delta^{18}O$ values, between +20.1 and +22.5‰, and $\delta^{13}C$ between +1.3 and +3.0‰. Therefore, most hydrothermal calcites have $\delta^{13}C$ within the range of the host limestones, with the exception of a few more depleted ore stage samples.

ORGANIC MATTER PETROLOGY AND GEOCHEMISTRY

Texture and reflectivity

Organic matter associated with the ore phases corresponds to black solid bitumen, of vitreous luster and concoidal fracture. The presence of degassing bubbles

and contraction cracks (Fig. 5D) reveals a previous fluid state. Some bitumen samples have μm-sized, round to elliptical patches, with higher reflectivity than the matrix. Random reflectivity measurements of bitumen (BR_O) were done in 13 samples (Table 3). In the samples with patches, only the reflectivity of the matrix was measured, except in sample ITX13-31, where the measurements were done randomly in both the matrix and patches, due to the abundance of the latter. Measured BR_O range from 0.76 to 3.24%, defining one single population (Fig. 7), and mean values of the individual samples are between 1.31 and 2.28% (Table 3). The highest BR_O values correspond to sample ITX13-31.

It is well known that the reflectivity of bitumen increases with thermal maturity and several correlations between BR_O and vitrinite reflectivity (VR_O) have been proposed (e.g., Jacob, 1989; Riediger, 1993; Landis and Castaño, 1995; Mort, 2004), resulting in different VR_O depending on the equation used. Applying the two extreme equations, the mean BR_O of the measured samples would correspond to VR_O between 0.99 and 1.5% using the equation of Mort (2004) ($BR_O = 1.9106\ VR_O - 0.5915$) while if the equation of Landis and Castaño (1995) is applied ($BR_O = 1.09\ VR_O - 0.41$), the VR_O would be between 1.58 and 2.47%. Consistent with these high reflectivity values, fluorescence was not observed in any sample.

Rock-Eval and hydrocarbon analysis

Rock-Eval analyses were done in 20 samples from the four boreholes (Table 3), including those with available reflectivity data. Six of the samples with low total organic carbon (TOC) contents (<0.7 wt. %) gave unreliable results (not listed in Table 3). Two other samples gave high T_{max} values (534 and 550°C) but they must be

considered unreliable because of flat S2 peaks. Therefore, the T_{max} range to be considered is comprised between 490 and 523ºC. Hydrogen index (HI) range from 16 to 145 mg HC/ g TOC and oil production index (OPI) from 0.03 to 0.34.

GC-MS analysis of the extractable hydrocarbon fractions was carried out on three samples (ITX13-4, ITX16-0 and ITX16-4) relatively poor in organic matter (TOC between 2 and 10.2 wt. %; Table 3). Sample ITX16-0, the richest in TOC and free hydrocarbons (S1 = 5.3 mg HC/ g rock) of the three, shows a n-alkane distribution extending up to nC_{35}, with a well-marked mode at nC_{15}-nC_{17} and a secondary one at nC_{25} and without any odd or even carbon number predominance (data not shown). The two other samples (ITX13-4 and ITX16-4) produced much narrower n-alkane distributions (between nC_{17} and nC_{30}) with a well marked maximum in the medium range (nC_{22} or nC_{23}) (data not shown). These three samples contain sulfur compounds (dibenzothiophenes) and sample ITX16-4 also contains low amounts of regular hopanes in C29 and C30.

Two samples of almost pure pyrobitumens (ITX13-31 and ITX28-3; 68.5 and 38.1 wt. % TOC, respectively) were submitted to hydrocarbon extraction and fractionation (Table 4) and to GC-MS analysis of saturates and aromatics, as well as to on-line py-GC-MS. The saturated hydrocarbon fraction of sample ITX13-31 displays a n-alkane distribution extending from nC_{17} to nC_{37}-nC_{38} without any odd or even preference and with a single mode at nC_{22} (Fig. 8). This sample also displays a notable hump of unresolved complex mixture (UCM), but without detectable common markers such as steranes and hopanes. The n-alkane distribution of sample ITX28-3, very rich in saturated hydrocarbons and without resins and asphaltenes (Table 4), extends only to nC_{32}-nC_{33}, also without any odd or even preference but with a major mode at nC_{18}-nC_{19}

and a secondary one at nC_{25} (Fig. 8). Sample ITX28-3 does not contain any sterane but a complete series of regular hopanes from C27 (Tm) to C35 (C28 lacking as a rule), with minor proportions of C27 and decreasing amounts towards the heavier compounds (Fig. 8). In the pyrolysates and in the corresponding free fractions, the same types of aromatic compounds were found. Only the pyrolysates are described next, since the lightest compounds were lost during solvent evaporation of the free fractions. In addition to a series of n-alkanes (much more abundant and heavier in ITX 13-31, mode at nC_{21}, than in ITX 28-3, mode at nC_{12}), py-GC-MS analyses revealed the presence of the following aromatic compounds in both samples: alkylbenzenes, naphtalenes, biphenyls, phenanthrenes and minor amounts of anthracenes, but also aromatic sulfur compounds such as dibenzothiophenes and minor proportions of benzonaphtothiophenes (Fig. 9 and Fig. 10). In all the compound series, the distributions are slightly displaced toward the lower ends in ITX 28-3 than in ITX 13-31, especially the n-alkanes, which show a much wider range than the aromatics. The implications of the hydrocarbon compositions and distributions on the analyzed samples will be discussed in the following section.

DISCUSSION

Organic matter origin, maturation and alteration processes

Studies related to organic matter in the BCB have considered various source rocks. Quesada et al., (1997) proposed the organic-rich Liassic black shales as the main source-rock for the Ayoluengo oil (the only onshore oil field in Spain; Fig. 1), and also for the whole BCB. However, Carboniferous coals could have also contributed to gas and/or oil production in the basin (Martínez del Olmo and Mallo, 2002) and, recently,

Agirrezabala et al. (2008) concluded that solid bitumen occurring within the Albian in an area near Itxaspe, was locally derived from organic-rich, Albian-Cenomanian Black Flysch Group facies.

The sole biomarkers that might be used to identify the source rock of the Itxaspe bitumen are the hopanes from sample ITX28-3. The distribution of normal hopanes in this sample is comparable to that of the Ayoluengo oil and its presumed source-rock (Quesada et al., 1997). However, the presence of the much more unusual and, thus, much more diagnostic diahopanes in C29 and C30 cannot be ascertained due to the important background of UCM (Fig. 8). The relatively high proportions of higher homologues (up to the C35) in the regular hopane distribution are probably derived from the bacteriohopanetetrol of anaerobes (e.g., Ourisson and Albrecht, 1992), revealing that the source rock was very probably deposited in marine euxinic conditions (e.g., Ramanampisoa and Disnar, 1994). Nevertheless, the n-alkane distribution extending towards the high molecular weight (beyond nC_{25}), suggests that this source rock also received terrestrial plant inputs, and thus, was probably deposited in a marginal setting.

All the considerations mentioned above, at first exclude the Carboniferous as the possible source rock of the bitumen. The choice between the two other formations, the Liasic and Albian-Cenomanian black shales, preferentially balances for the nearest one, since a long migration distance of small bitumen amounts is expected to provoke much greater compositional changes than those observed in the bitumen from Itxaspe (Hu et al., 1998). From the local geology it can be inferred that the nearest source rock was the Albian-Cenomanian black shales (EVE, 1995).

The presence of notable proportions of aromatic sulfur-bearing compounds in the studied bitumen samples is consistent either with: (a) a source rock deposited in marine euxinic conditions, where they are formed by early diagenetic sulfurization processes (e.g., Ho et al., 1974); and/or (b) the participation of organic matter in TSR (e.g., Manzano et al., 1997; Ding et al., 2008; Zhang et al., 2008). The exclusive presence of highly aromatic sulfur compounds, such as dibenzothiophenes (Fig. 9 and Fig. 10), is consistent with the high maturity of the bitumen, which favors the formation of these compounds at the expense of their less stable precursors, such as benzothiophenes (Ho et al., 1974; Mueller et al., 1995). Benzonaphtothiophenes can be considered as higher homologues of dibenzothiophenes.

The variable compositions of the bitumen samples from Itxaspe clearly indicate that they underwent different alteration processes. However, the presence of notable proportions of n-alkanes, well-known as the first type of hydrocarbons to be affected by biodegradation, suggests that they were not affected by this process and, consequently, that they were not involved in BSR. The two samples analyzed in more detail, ITX13-31 and ITX28-3, reached the same degree of maturity (T_{max} of 505 and 504°C, respectively) and, therefore, their compositional differences may be attributed to other alteration processes. Sample ITX28-3 is slightly richer in free hydrocarbons and hydrogen than ITX13-31 (S1 and HI values in Table 3), consistent with the greater proportions of naphtenes responsible for the UCM hump in the free saturated hydrocarbon fraction, especially in the high molecular weight range (i.e. where the peaks of hopanes appear; Fig. 8). The differences in their n-alkane abundances can be related to a fractionation during expulsion and/or migration of hydrocarbons, favoring the migration of acyclic compounds over cyclic and aromatic ones (Hu et al, 1998;

Eseme et al., 2007 and references therein). Accordingly, the differences in composition of the two bitumen samples could tentatively be explained by a greater migration distance of bitumen from sample ITX13-31.

T_{max} values can be considered a reliable maturity index for asphaltenes (and by extension for bitumens) as they are for kerogens (Nali et al., 2000). At Itxaspe, T_{max} (490-523ºC), OPI values (up to 0.34; Table 3), and calculated VR_O (up to 2.5%), indicate that the organic matter reached the gas window. The low HI values (up to 145 mg HC/ g TOC; Table 3) could be the result of organic matter maturation, in consistence with the low HI value (45 mg HC/ g TOC) of the overmatured type I/II sample reported by Quesada et al. (1997). Moreover, TSR could also contribute to the hydrogen loss (Leventhal, 1990).

Sulfate reduction processes and the role of organic matter

Based on crush-leach and stable isotope data, the ultimate source of sulfur in the Itxaspe mineralization is considered to be Mesozoic marine and/or evaporite sulfate. $\delta^{34}S$ of sphalerite from Itxaspe show a wide range (+3.5 to +17.7‰), which is similar to those found in other Zn-Pb deposits from the BCB (Herrero, 1989; Velasco et al., 1994, 2003; Perona et al., 2007). These authors interpreted the variations of $\delta^{34}S$ as a result of mixing of fluids with different $\delta^{34}S$, different reduction mechanisms, or a combination of both.

The reduction of aqueous sulfate to produce H_2S can occur either biologically (BSR) or abiologically (TSR). Based on empirical evidences, BSR and TSR occur in two mutually exclusive thermal regimes: BSR regimes are generally characterized by temperatures below ca. 80ºC, although hyperthermophilic sulfate-reducing bacteria may

persist to temperatures up to 110ºC (e.g., Jørgensen et al., 1992). In contrast, TSR rates are significant at higher temperatures (see citations in Cross et al., 2004).

Sulfate reduction processes in natural systems tend to have characteristic, kinetically controlled, non-equilibrium isotope fractionation factors: Goldhaber and Kaplan (1975) reported fractionation factors for sulfur from 15 to 60‰ during BSR in marine settings. During TSR, the kinetic sulfur fractionation is about 20‰ at 100ºC, about 15‰ at 150ºC and about 10‰ at 200ºC (Kiyosu and Krouse, 1990). The range of $\delta^{34}S$ in sphalerite from Itxaspe is compatible with both BSR and TSR in a system partially closed to sulfate. If there is limited availability of sulfate during the reduction process, the $\delta^{34}S$ of the resulting H_2S will be lighter at the beginning and will turn heavier with time. The $\delta^{34}S$ and $\delta^{18}O$ of some barites (up to +23.1‰ and +17.8‰, respectively) point to the precipitation from a residual, ^{34}S- and ^{18}O-enriched sulfate, which is consistent with this hypothesis.

If BSR-derived H_2S was involved in sulfide formation, the reduction process necessarily took place before, or at some distance from the mineralization site, since ore stage brine temperatures (T_h ~130ºC) were too high for BSR to succeed. Framboidal pyrite found in the mineralization host rocks suggests that BSR took place before the onset of the hydrothermal event, therefore, some (or even all) the reduced sulfur generated during this episode of BSR was trapped in the form of pyrite, while any residual H_2S could either remain at the site or migrate. The elapsed time between this BSR episode and the onset of the mineralizing event is unknown. Nevertheless, as quoted in the previous section, the analyzed bitumen from Itxaspe was most likely not involved in any BSR process.

Ore stage brine temperatures are compatible with a TSR of the sulfate dissolved in the mineralizing fluid. Reduced sulfur species, such as H_2S, are essential for TSR to take place (e.g., Toland, 1960) and thermal cracking of crude oil can generate small amounts of H_2S (generally <5% of total gas volume; Orr, 1977). Therefore, the maturation of organic matter produced by the hydrothermal brines could be the first process involved in the generation of H_2S in Itxaspe, needed for triggering TSR.

Itxaspe bitumens may either have formed by polymerization during TSR or as by-product of thermal cracking. In natural environments with crude oil and/or wet gas as the carbon source, TSR can generate naphthenic acids, aromatic compounds, solid bitumen and numerous inorganic and organic sulfur compounds such as polysulfides, mercaptans, thialkenes and thiophenes (e.g., Machel, 2001). Therefore, the aromatic sulfur compounds (or their less stable precursors) present in the bitumen samples from Itxaspe, and the solid bitumen itself, could have been produced during TSR.

The absence of clearer molecular evidence of TSR (such as the presence of bridgehead 2-thiaadamantanes; Hanin et al., 2002) is consistent with recent experiments by Zhang et al. (2007), who demonstrated that hydrocarbon chemistry only exerts a limited control on TSR. Nevertheless, this general conclusion is somewhat in contradiction with an apparent greater reactivity of compounds such as the isoprenoids pristane and phytane (Zhang et al., 2008). The almost or even total absence of these isoprenoids in the five studied samples from Itxaspe is noteworthy, since these compounds can be highly concentrated during oil migration as highlighted by previous findings in the BCB (Hu et al., 1998). Accordingly, it can be suspected that these compounds were here consumed during TSR.

A temperature decrease during the late stages of the mineralization would lead to a significant reduction of the TSR reaction rate and, thus, of the amount of H_2S produced (e.g., Thom and Anderson, 2008), contributing to the end of the sulfide precipitation. Another possibility would be the depletion of the reducing agent (organic matter) itself. However, sulfate was not yet exhausted, since at the end of the sulfide ore stage barite continued to precipitate.

CONCLUSIONS

The study of the Itxaspe Zn-(Pb) occurrence in the Mississippi Valley-type district of the Basque-Cantabrian basin (N Spain) has provided evidence of a close link between organic matter oxidation and ore formation. Measured temperatures in the ore forming brines are compatible with a TSR process with organic matter as the reducing agent. The close petrographic relationship between ore and bitumen, the presence of organo-sulfur compounds and the $\delta^{34}S$ of the precipitated sulfides and sulfates are consistent with TSR. The origin of dissolved solutes (including sulfate) in the ore fluids is related to the dissolution of Triassic evaporite units, without ruling out the contribution of evaporated seawater brines. The source rock of the bitumen associated with the ore phases was very probably deposited in marine euxinic conditions, but in a marginal setting. The differences in composition of the bitumen samples can be related to a fractionation during expulsion and/or migration of hydrocarbons. From all these data, it can be suggested that in situ TSR during ore formation is a plausible mechanism for providing the necessary reduced sulfur involved in the ore genesis, at least for small Zn-Pb mineralizations like Itxaspe.

ACKNOWLEDGEMENTS

This work has been financed through a CICYT project (BTE2003-01346) and an Acción Integrada Hispano-Francesa (HF2005-0036) from the Spanish Ministry of Education and Science. À. P. has benefited from the FPU program from the same ministry. The authors wish to thank the EVE, especially J. García, for supplying the drill core samples, D. Banks for his assistance during the crush-leach analyses, F. Laggoun-Defarge for her help during the bitumen reflectivity measurements and E. Cardellach for carefully reviewing an earlier version of the manuscript. We are also grateful to G.M. Anderson and A. Gize for their constructive reviews of the manuscript.

REFERENCES

Agirrezabala, L.M., Dorronsoro, C., Permanyer, A., 2008. Geochemical correlation of pyrobitumen fills with host mid-Cretaceous Black Flysch Group (Basque-Cantabrian Basin, western Pyrenees). Organic Geochemistry, 38(8), 1185-1188.

Bakker, R.J., 2003. Package FLUIDS 1. Computer programs for analysis of fluid inclusion data and for modelling bulk fluid properties. Chemical Geology, 194(1-3), 3-23.

Banks, D.A., Giuliani, G., Yardley, B.W.D., Cheilletz, A., 2000. Emerald mineralisation in Colombia: fluid chemistry and the role of brine mixing. Mineralium Deposita, 35(8), 699-713.

Barbanson, L., 1987. Les gisements Zn, Pb, Ba, Hg, Cu de socle et de couverture carbonatés de la province de Santander (Nord de l'Espagne). Thèse d'Etat. Université d'Orléans.

Bodnar, R.J., 1993. Revised equation and table for determining the freezing point depression of H_2O-NaCl solutions. Geochimica et Cosmochimica Acta, 57(3), 683-684.

Boyce, A.J., Fallick, A.E., Hamilton, P.J., Elorza, J., 1990. Diagenesis of celestite in quartz geodes from the Basque-Cantabric basin, Northern Spain: Evidence from sulphur and strontium isotopes. Chemical Geology, 84(1-4), 354-356.

Bustillo, M., Ordóñez, S., 1995. Lower Cretaceous Pb-Zn ores of Cantabria, Northern Spain: New considerations based on petrological and geochemical evidence. Transactions of Institution of Mining and Metallurgy, 104, B55-B65.

Carracedo, M., Larrea, F.J., Alonso, A., 1999. Estructura y organización de las coladas submarinas: características de las lavas almohadilladas de edad Cretácica que afloran en la cordillera Vasco-Cantábrica. Estudios Geológicos, 55, 209-222.

Charef, A., Sheppard, S.M.F., 1984. Carbon and oxigen isotope analysis of calcite or dolomite associated with organic matter. Isotope Geoscience, 2, 325-333.

Claypool, G.E., Holser, W.T., Kaplan, I.R., Sakai, H., Zak, I., 1980. The age curves of sulfur and oxygen isotopes in marine sulfate and their mutual interpretations. Chemical Geology, 28, 199-260.

Cross, M.M., Manning, D.A.C, Bottrell, S.H., Worden, R.H., 2004. Thermochemical sulphate reduction (TSR): experimental determination of reaction kinetics and implications of the observed reaction rates for petroleum reservoirs. Organic Geochemistry, 35(4), 393-404.

Davis, D.W., Lowenstein, T.K., Spencer, R.J., 1990. Melting behavior of fluid inclusions in laboratory-grown halite crystals in the systems NaCl-H_2O, NaCl-KCl-H_2O, NaCl-$MgCl_2$-H_2O and NaCl-$CaCl_2$-H_2O. Geochimica et Cosmochimica Acta, 54(3), 591-601.

Ding, K., Li, S., Yue, C., Zhong, N., 2008. A simulation on the formation of organic sulfur compounds in petroleum from thermochemical sulfate reduction. Journal of Fuel Chemistry and Technology, 36(1), 48-54.

Disnar, J.R., 1996. A comparison of mineralization histories for two MVT deposits, Trèves and Les Malines (Causses basin, France), based on the geochemistry of associated organic matter. Ore Geology Reviews, 11(1-3), 133-156.

Eseme, E., Littke, R., Krooss, B.M., Schwarzbauer, J., 2007. Experimental investigation of the compositional variation of petroleum during primary migration. Organic Geochemistry, 38(8), 1373–1397.

EVE, 1995. Mapa geológico del País Vasco. Scale 1:100.000. Ente Vasco de la Energía. 345 pp., 1 fold. map.

Fernández-Martínez, J., Velasco, F., 1996. The Troya Zn-Pb carbonate-hosted sedex deposit, Northern Spain. In: Sangster, D.F. (ed.). Carbonate hosted lead-zinc deposits. Society of Economic Geologists Special Publication, 4, 364-377.

Fontes, J.Ch., Matray, J.M., 1993. Geochemistry and origin of formation brines from the Paris Basin, France: 1. Brines associated with Triassic salts. Chemical Geology, 109(1-4), 149-175.

García-Mondéjar, J., 1989. Strike-slip subsidence of the Basque-Cantabrian Basin of northern Spain and its relationship to Aptian-Albian opening of the Bay of Biscay. In: Tankard, A.J., Balkwill, H.R. (eds.). Extensional tectonics and stratigraphy of the North Atlantic margins. AAPG memoir, 46, 395-409.

García-Mondéjar, J., 1990. The Aptian-Albian carbonate episode of the Basque-Cantabrian Basin (Northern Spain): General characteristics, controls and evolution. In: Tucker, M. (ed.). Carbonate platform and basin sedimentary systems. International Association of Sedimentologists Special Publication, 9, 257-290.

García-Mondéjar, J., Agirrezabala, L.M., Aranburu, A., Fernández-Mendiola, P.A., Gómez-Pérez, I., López-Horgue, M., Rosales, I., 1996. Aptian-Albian tectonic pattern of the Basque-Cantabrian Basin (Northern Spain). Geological Journal, 31(1), 13-45.

Gil, P.P., 1991. Las mineralizaciones de hierro del Anticlinal de Bilbao: Mineralogía, geoquímica y metalogenia. Doctoral Thesis. Universidad del País Vasco, 343 pp.

Goldhaber, M.B., Kaplan, I.R., 1975. Controls and consequences of sulfate reduction rates in recent marine sediments. Soil Science, 119(1), 42-55.

Gómez, M., Vergés, J., Riaza, C., 2002. Inversion tectonics of the northern margin of the Basque Cantabrian Basin. Bulletin de la Société Géologique de France, 173(5), 449-459.

Grandia, F., Canals, À., Cardellach, E., Banks, D.A., Perona, J., 2003. Origin of ore-forming brines in sediment-hosted Zn-Pb deposits of the Basque-Cantabrian Basin, Northern Spain. Economic Geology, 98(7), 1397-1411.

Hanin, S., Adam, P., Kowalewski, I., Huc, A.Y., Carpentier, B., Albrecht, P., 2002. Bridgehead alkylated 2-thiaadamantanes: novel markers for sulfurization processes occurring under high thermal stress in deep petroleum reservoirs. Chemical Communications, 16, 1750–1751.

Herrero, J.M., 1989. Las mineralizaciones de Zn, Pb, F en el sector occidental de Vizcaya: Mineralogía, geoquímica y metalogenia. Doctoral Thesis. Universidad del País Vasco, 285 pp.

Ho, T.Y., Rogers, M.A., Drushel, H.V., Koons, C.B., 1974. Evolution of sulfur compounds in crude oils. The American Association of Petroleum Geologists Bulletin, 58(11), 2338-2348.

Hu, M.A., Disnar, J.R., Barbanson, L., Suarez-Ruiz, I., 1998. Processus d'altération thermique, physico-chimique et biologique de constituants organiques et genèse d'une minéralisation sulfurée: le gîte Zn-Pb de La Florida (Cantabria, Espagne). Canadian Journal of Earth Sciences, 35(8), 936-950.

IGME-EVE, 2000. Mapa Metalogenético del País Vasco. Scale 1:1,000,000. Unpublished report.

International Committee for Coal Petrology, 1971. International handbook of coal petrography, 2nd ed. Paris, CNRS.

Jacob, H., 1989. Classification, structure, genesis and practical importance of natural solid oil bitumen ("migrabitumen"). International Journal of Coal Geology, 11(1), 65-79.

Jørgensen, B.B., Isaksen, M.F., Jannasch, H.W., 1992. Bacterial sulfate reduction above 100ºC in deep sea hydrothermal vent sediments. Science, 258 (5089), 1756-1757.

Kesler, S.E., Jones, H.D., Furman, F.C., Sassen, R., Anderson, W.H., Kyle J.R., 1994. Role of crude oil in the genesis of Mississippi Valley-type deposits: Evidence from the Cincinnati arch. Geology, 22(7), 609-612.

Kiyosu, Y., Krouse, H.R., 1990. The role of organic acid in the abiogenic reduction of sulfate and the sulfur isotope effect. Geochemical Journal, 24(1), 21-27.

Lafargue, E., Marquis, F., Pillot, D., 1998. Rock-Eval 6 applications in hydrocarbon exploration, production and soil contamination studies. Revue de l'Institut Français du Pétrole, 53(4), 421-437.

Landis, C.R., Castaño, J.R., 1995. Maturation and bulk chemical properties of a suite of solid hydrocarbons. Organic Geochemistry, 22(1), 137-149.

Leventhal, J.S., 1990. Organic matter and thermochemical sulfate reduction in the Viburnum Trend, southeast Missouri. Economic Geology, 85(3), 622-632.

Machel, H.G., 2001. Bacterial and thermochemical sulfate reduction in diagenetic settings – old and new insights. Sedimentary Geology, 140(1-2), 143-175.

Manzano, B.K., Fowler, M.G., Machel, H.G., 1997. The influence of thermochemical sulphate reduction on hydrocarbon composition in Nisku reservoirs, Brazeau river area, Alberta, Canada. Organic Geochemistry, 27(7-8), 507-521.

Martínez del Olmo, W., Mallo, J.M., 2002. Non-renewable energy resources: oil and gas. In: Gibbons, W., Moreno, T. (eds.). Geology of Spain. Blackwell, 494–499.

Mort, A., 2004. Mécanismes de formation et évolution des pyrobitumes dans les réservoirs pétroliers : cas naturels et approches expérimentales. Doctoral Thesis. Université d'Orléans, 248 pp.

Mueller, E., Philp, R.P., Allen, J., 1995. Geochemical characterization and relationship of oils and solid bitumens from SE Turkey. Journal of Petroleum Geology, 18(3), 289-308.

Nali, M. Caccialanza, G., Ghiselli, C., Chiaramonte, M.A., 2000. T_{max} of asphaltenes: a parameter for oil maturity assessment. Organic Geochemistry, 31(12), 1325-1332.

Oakes, C.S., Bodnar, R.J., Simonson, J.M., 1990. The system NaCl-$CaCl_2$-H_2O: I. The ice liquidus at 1 atm total pressure. Geochimica et Cosmochimica Acta, 54(3), 603-610.

Orr, W.L., 1977. Geologic and geochemical controls on the distribution of hydrogen sulfide in natural gas. In: Campos, R., Goni, J. (eds). Advances in Organic Geochemistry. Enadisma, Madrid, 571-597.

Ourisson, G., Albrecht, P., 1992. Hopanoids . 1. Geohopanoids: the most abundant natural product on Earth? Accounts of Chemical Research, 25(9), 398–402.

Outokumpu-EVE, 1995. Campaña de sondeos en el P.I. Andutz. Area de Itxaspe. Unpublished report.

Perona, J., Cardellach, E., Canals, À., 2007. Origin of diapir-related Zn-Pb deposits in the Basque-Cantabrian Basin (Northern Spain). In: Andrew, C.J. et al. (eds). Digging Deeper, vol. 2. Proceedings of the ninth biennial SGA meeting, Dublin. Irish Association for Economic Geology, 1303-1306.

Perona, J., Disnar, J.R., Laggoun-Défarge, F., Canals, À., 2004. Estudio de la materia orgánica asociada a depósitos peridiapíricos de Zn-Pb de la cuenca Vasco-Cantábrica. Macla, 2, 39-40.

Powell, T.G., Macqueen, R.W., 1984. Precipitation of sulfide ores and organic matter: sulfate reactions at Pine Point, Canada. Science, 224(1), 63-66.

Quesada, S., Dorronsoro, C., Robles, S., Chaler, R., Grimalt, J.O., 1997. Geochemical correlation of oil from the Ayoluengo field to Liassic black shale units in the southwestern Basque-Cantabrian Basin (northern Spain). Organic Geochemistry, 27(1-2), 25-40.

Ramanampisoa, L., Disnar, J.R., 1994. Primary control of paleoproduction on organic matter preservation and accumulation in the Kimmeridge rocks of Yorkshire (UK). Organic Geochemistry, 21(12), 1153-1167.

Rat, P., 1987. The Basque-Cantabrian basin between the Iberian and European plates: Some facts but still many problems. Revista de la Sociedad Geológica de España, 1(3-4), 327-348.

Riediger, C.L., 1993. Solid bitumen reflectance and Rock-Eval T_{max} as maturation indices: an example from "Nordegg Member", Western Canada Sedimentary Basin. International Journal of Coal Geology, 22(3-4), 295-315.

Selby, D., Creaser, R.A., Dewing, K., and Fowler, M., 2005. Evaluation of bitumen as a ^{187}Re-^{187}Os geochronometer for hydrocarbon maturation and migration: A test case from the Polaris MVT deposit, Canada. Earth and Planetary Science Letters, 235(1-2), 1-15.

Simón, S., Canals, À., Grandia, F., Cardellach, E., 1999. Estudio isotópico y de inclusiones fluidas en depósitos de calcita y dolomita del sector oeste del Anticlinal de Bilbao y su relación con las mineralizaciones de Fe-Zn-Pb. Boletín de la Sociedad Española de Mineralogía, 22, 55-71.

Spangenberg, J.E., Macko, S.A., 1998. Organic geochemistry of the San Vicente zinc-lead district, eastern Pucará Basin, Peru. Chemical Geology, 146(1-2), 1-23.

Thom, J., Anderson, G.M., 2008. The role of thermochemical sulfate reduction in the origin of Mississippi Valley-type deposits. I. Experimental results. Geofluids, 8(1), 16-26.

Toland, W.G., 1960. Oxidation of organic compounds with aqueous sulfate. Journal of the American Chemical Society, 82(8), 1911-1916.

Velasco, F., Herrero, J.M., Gil, P.P., Álvarez, L., Yusta, I., 1994. Mississippi Valley-type, Sedex and iron deposits in lower Cretaceous rocks of the Basque-Cantabrian basin, Northern Spain. In: Fontboté, L., Boni, M. (eds.). Sediment-hosted Zn-Pb ores. Society for Geology Applied to Mineral Deposits Special Publication, 10, 246-270.

Velasco, F., Herrero, J.M., Yusta, I., Alonso, J.A., Seebold, I., Leach, D., 2003. Geology and geochemistry of the Reocín zinc-lead deposit, Basque-Cantabrian basin, Northern Spain. Economic Geology, 98(7), 1371-1396.

Zhang, T., Ellis, G.S., Walters, C.C., Kelemen, S.R., Wang, K., Tang, Y., 2008. Geochemical signatures of thermochemical sulfate reduction in controlled hydrous pyrolysis experiments. Organic Geochemistry, 39(3), 308–328.

Zhang, T., Ellis, G.S., Wang, K., Walters, C.C., Kelemen, S.R., Gillaizeau, B., Tang, Y., 2007. Effect of hydrocarbon type on thermochemical sulfate reduction. Organic Geochemistry, 38(6), 897-910.

Figure captions

Figure 1. Simplified geological map of the Basque-Cantabrian region (from García-Mondéjar et al., 1996), with the location of the Itxaspe Zn-(Pb) mineralization, of other Zn-Pb and Fe deposits and of oil and gas fields.

Figure 2. Geological map of the area around Itxaspe (Outokumpu-EVE, 1995), with the locations of the sampled boreholes, and drill core description. The position of the studied samples in the drill cores is also shown.

Figure 3. Drill core samples of different host rocks and mineralization styles. Scale bar is 1 cm. (A) Silicified breccia with disseminated sphalerite in the matrix (sample ITX13-1). (B) White calcite and disseminated sphalerite replacing the limestone (sample ITX16-4). (C) Massive sphalerite, with minor barite (grey) in the upper left part (sample ITX13-3). (D) Silicified breccia with veinlets of sphalerite, calcite, barite and quartz (sample ITX16-6).

Figure 4. Paragenetic sequence of the Itxaspe Zn-(Pb) mineralization.

Figure 5. Microscopic images under transmitted light. Scale bar is 500 μm. (A) Zoned, brown sphalerite, together with calcite (cal) and fine-grained quartz (qtz) (sample ITX16-2). (B) Brown sphalerite crystals crosscut by a late, honey-colored sphalerite vein (sample ITX20-1). (C) Sample with euhedral quartz crystals (central part) containing bitumen in growth bands (see arrows) and in contact with black solid bitumen patches (sample ITX16-7). (D) Black solid bitumen patch with degassing

bubbles and contraction cracks, now filled with calcite. Brown phase is sphalerite (sample ITX13-3). (E) Barite crystals in fan-shaped aggregates (grey), together with calcite (sample ITX16-5). (F) Sphalerite (brown) and bournonite (black) crystals partially or completely replaced by late quartz (white). See arrows pointing to some of the replaced crystals. The matrix is made up of quartz and phyllosilicates (sample ITX16-2).

Fig. 6. (A) Histogram of ice melting temperatures and (B) histogram of homogenization temperatures of fluid inclusions in sphalerite from Itxaspe.

Figure 7. Histogram of bitumen reflectivity data from Itxaspe.

Figure 8. Partial reconstructed chromatograms (TIC) of the saturated hydrocarbon fractions of samples ITX 13-31 and ITX 28-3 and distribution of hopanes in sample ITX 28-3, evidenced by selective m/z 191 ion detection. IS1= internal standard (squalane). nCx = n-alkane. Cx = regular hopane; D? = possible diahopane in C29.

Figure 9. Partial reconstructed chromatogram (TIC) of the on-line pyrolysate of sample ITX 13-31 and distribution of the major series of constituents recognized by selective ion detection. IS1 and IS2 = internal standards (squalane and α-cholestane, respectively). nCx = n-alkane.

Figure 10. Partial reconstructed chromatogram (TIC) of the on-line pyrolysate of sample ITX 28-3 and distribution of the major series of constituents recognized by

selective ion detection. IS1 and IS2 = internal standards (squalane and α-cholestane, respectively). nCx = n-alkane.

TABLE 1. Leachate analyses of fluid inclusions from Itxaspe, as measured concentrations (in ppb) and as molar ratios.

Sample	Mineral	Cl^-	Br^-	Na^+	K^+	Li^+	Cl/Br	Na/Br	Na/Li	Na/K
ITX13-3	Sphalerite	6957.8	10.4	4704	13892	38.6	1506	1570	14	0.6
ITX16-4	Sphalerite	7662.9	12.9	3549	3122	99.2	1341	957	86	2
ITX16-4	Late stage calcite	46823.7	90.5	18868	1493	12.5	1166	725	147	21

TABLE 2. Stable isotope data for sulfide, sulfate and carbonate samples from Itxaspe.

Sample	Mineral	Description	$\delta^{34}S$ (‰ VCDT)	$\delta^{18}O$ (‰ VSMOW)	$\delta^{13}C$ (‰ VPDB)
ITX13-3	Sphalerite	Massive	+5.3		
ITX16-1	Sphalerite	Disseminated	+9.5		
ITX16-2a	Sphalerite	Disseminated	+8.1		
ITX16-3	Sphalerite	Disseminated	+7.3		
ITX16-4	Sphalerite	Disseminated	+3.5		
ITX16-5b	Sphalerite	Disseminated	+10.9		
ITX16-6	Sphalerite	In vein	+9.6		
ITX16-7	Sphalerite	Disseminated	+8.7		
ITX20-1	Sphalerite	Massive	+17.7		
ITX20-2	Sphalerite	Disseminated	+6.6		
ITX28-1	Sphalerite	Disseminated	+5.8		
ITX28-1	Galena	Disseminated	+3.3		
ITX13-2b	Barite	Massive (late stage)	+22.3	+17.2	
ITX13-3	Barite	Disseminated (late stage)	+23.1	+17.8	
ITX16-1	Barite	In fracture (late stage)	+22.4	+15.8	
ITX16-5a	Barite	Replacement (late stage)	+18.3	+15.6	
ITX13-1	Calcite	In vein (ore stage)		+18.06	-0.49
ITX13-2b	Calcite	In vein (ore stage)		+17.80	+2.09
ITX13-4	Calcite	In vein (late stage)		+20.10	+3.02
ITX13-4	Calcite	Host limestone		+25.63	+3.03
ITX16-2	Calcite	Host limestone		+26.85	+3.48
ITX16-2a	Calcite	Ore stage		+20.40	+3.60
ITX16-3	Calcite	In vein (ore stage)		+18.99	+3.11
ITX16-3	Calcite	Host limestone		+21.20	+2.40
ITX16-4	Calcite	Replacement (late stage)		+21.42	+2.58
ITX16-4	Calcite	Host limestone		+24.34	+2.72
ITX16-5	Calcite	In vein (late stage)		+20.97	+1.32
ITX16-7	Calcite	In vein (late stage)		+20.36	+1.58
ITX20-1	Calcite	In vein (ore stage)		+19.72	-1.68
ITX20-2	Calcite	Host limestone		+24.84	+3.12
ITX28-2	Calcite	In vein (late stage)		+22.52	+2.93
ITX28-3	Calcite	In cavity (late stage)		+20.65	+1.35

TABLE 3. Bitumen reflectivity (BR_O) and Rock-Eval results from Itxaspe samples.

Sample	Lithology	Reflectivity				TOC	S1	S2	T_{max}	HI	OICO	OI	OPI
		Min.	Max.	Mean	n	(wt. %)	(mg HC/g rock)	(mg HC/g rock)	(ºC)	(mg HC/g TOC)	(mg CO/ g TOC)	(mg CO_2/ g TOC)	(S1/ (S1+S2))
ITX13-1	Breccia					0.61	0.03	0.1	517	16	8	34	0.22
ITX13-3	Breccia	0.758	1.768	1.314	89	1.2	0.05	0.32	502	27	2	10	0.14
ITX13-31	Bitumen	1.966	3.063	2.282	209	68.49	7.7	73.89	505	108	1	2	0.09
ITX13-4a	Limestone	1.627	2.224	1.945	119	2.31	0.21	1.28	516	55	3	9	0.14
ITX13-4b	Limestone	1.191	2.164	1.740	160								
ITX16-0	Barite + bitumen in vein					10.19	5.27	10.35	490	102	1	3	0.34
ITX16-1	Breccia					1.78	0.31	1.41	497	79	15	19	0.18
ITX16-2b	Bitumen in vein	1.055	1.829	1.524	101								
ITX16-4	Bitumen in vein	1.480	2.278	1.820	200	1.96	0.27	1.39	513	71	2	15	0.16
ITX16-5	Breccia					0.64	0.02	0.16	523	25	12	42	0.09
ITX16-6	Breccia					0.23	0.02	0.08	488	35	0	39	0.22
ITX16-7	Breccia	1.656	2.059	1.896	31	0.8	0.03	0.2	534	25	14	32	0.12
ITX20-1a	Breccia	1.408	2.204	1.981	93	0.23	0.03	0.15	519	65	43	61	0.16
ITX20-1b	Massive ore	1.157	2.094	1.510	105								
ITX20-2	Breccia	1.723	2.025	1.893	30								
ITX28-1	Breccia	1.763	2.103	1.980	30	5.83	0.06	2.04	550	35	4	5	0.03
ITX28-2a	Breccia	1.325	2.078	1.726	108	0.47	0.04	0.17	501	36	4	23	0.2
ITX28-3	Bitumen in cavity	1.294	3.236	1.955	208	36.08	11.39	52.35	504	145	1	1	0.18

TABLE 4. Composition of the extractable hydrocarbon fraction of bitumen samples ITX13-31 and ITX28-3.

Sample	Extract		Asphaltens	Resins	Saturates	Aromatics
	(mg/g sed.)	(mg/g TOC)	(%)	(%)	(%)	(%)
ITX13-31	0.93	1.36	18.2	13.6	31.8	36.4
ITX28-3	0.77	2.13	0	0	66.7	33.3

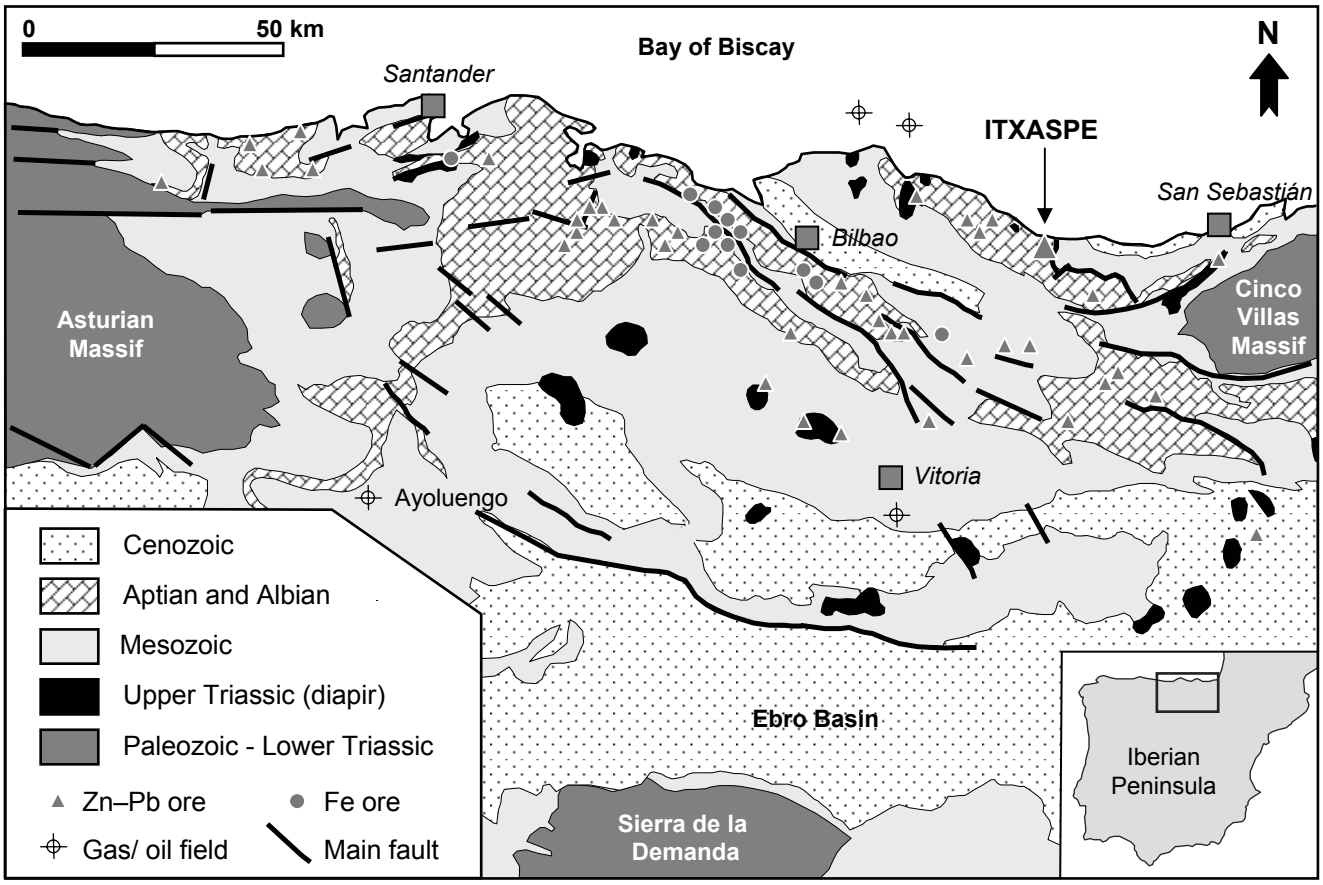
0
50 km
Bay of Biscay
N
Santander
ITXASPE
San Sebastián
Bilbao
Asturian Massif
Cinco Villas Massif
Vitoria
Ayoluengo
Cenozoic
Aptian and Albian
Mesozoic
Upper Triassic (diapir)
Paleozoic - Lower Triassic
Zn–Pb ore
Fe ore
Gas/ oil field
Main fault
Ebro Basin
Iberian Peninsula
Sierra de la Demanda

Figure 1

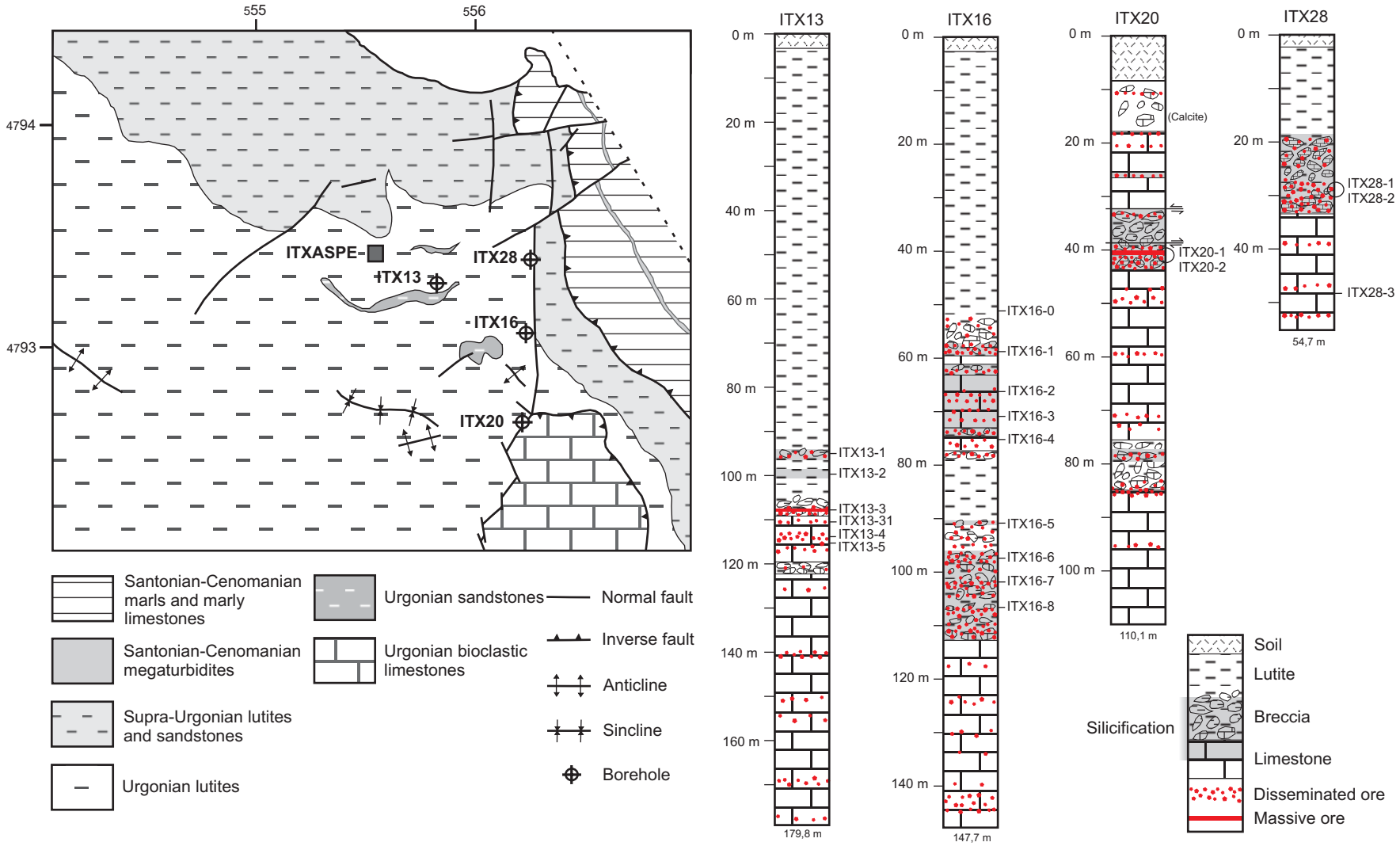
555
556
4794
4793
ITXASPE
ITX13
ITX28
ITX16
ITX20
Santonian-Cenomanian marls and marly limestones
Santonian-Cenomanian megaturbidites
Supra-Urgonian lutites and sandstones
Urgonian lutites
Urgonian sandstones
Urgonian bioclastic limestones
Normal fault
Inverse fault
Anticline
Sincline
Borehole
ITX13
ITX13-1
ITX13-2
ITX13-3
ITX13-31
ITX13-4
ITX13-5
179,8 m
ITX16
ITX16-0
ITX16-1
ITX16-2
ITX16-3
ITX16-4
ITX16-5
ITX16-6
ITX16-7
ITX16-8
147,7 m
ITX20
(Calcite)
ITX20-1
ITX20-2
110,1 m
ITX28
ITX28-1
ITX28-2
ITX28-3
54,7 m
Soil
Lutite
Breccia
Limestone
Disseminated ore
Massive ore
Silicification

Figure 2

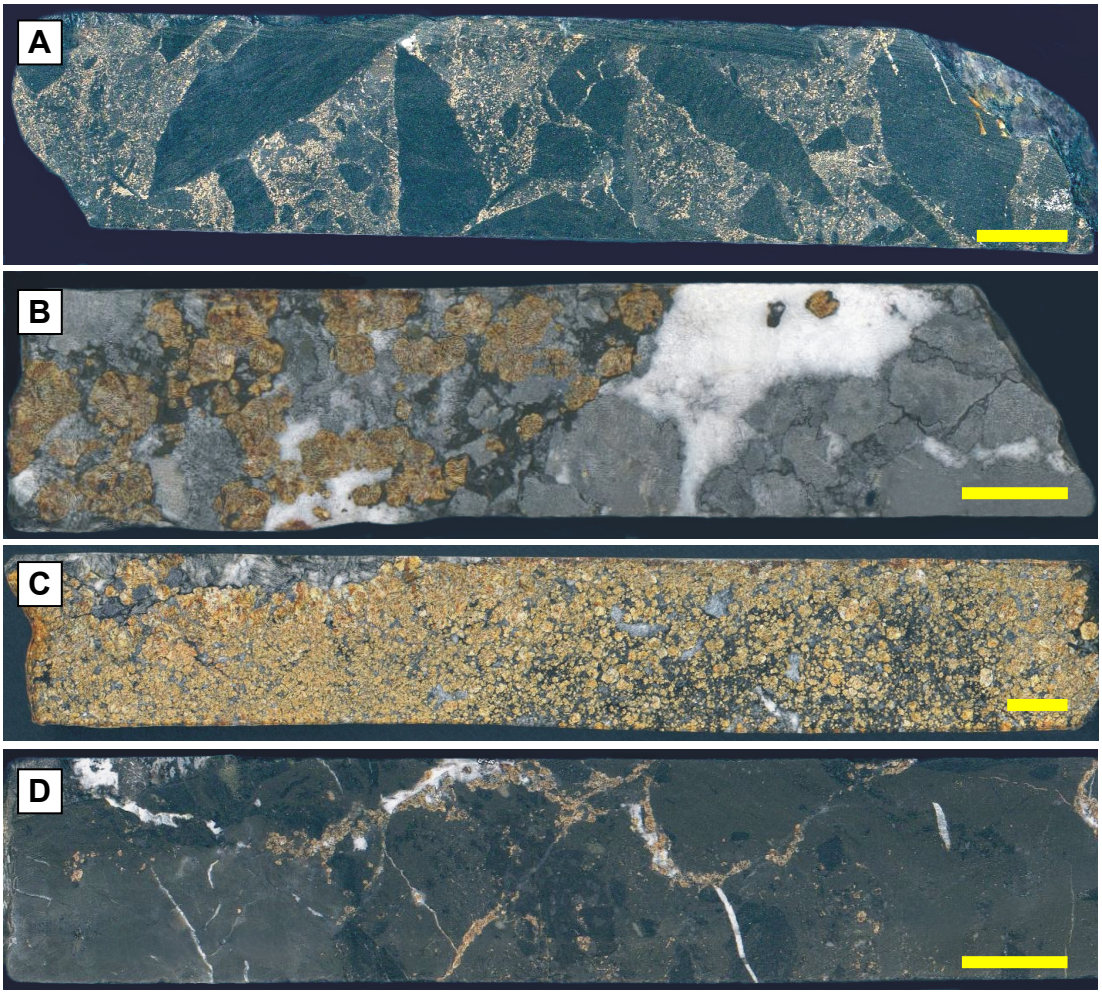

Figure 3

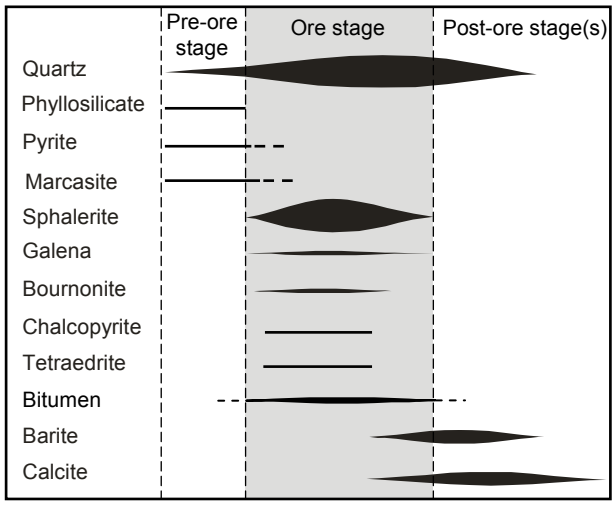
Pre-ore stage
Ore stage
Post-ore stage(s)
Quartz
Phyllosilicate
Pyrite
Marcasite
Sphalerite
Galena
Bournonite
Chalcopyrite
Tetraedrite
Bitumen
Barite
Calcite

Figure 4

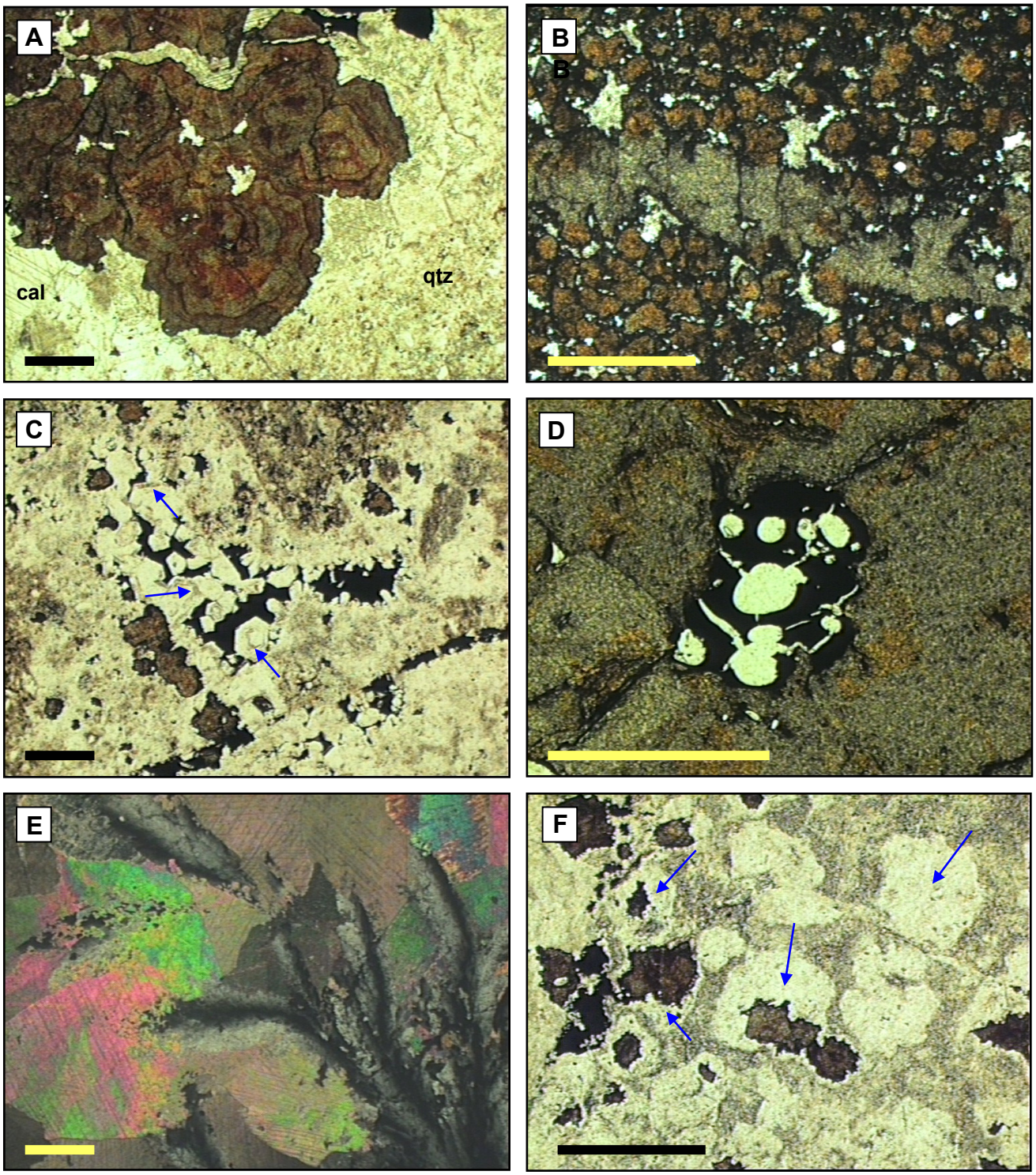

Figure 5

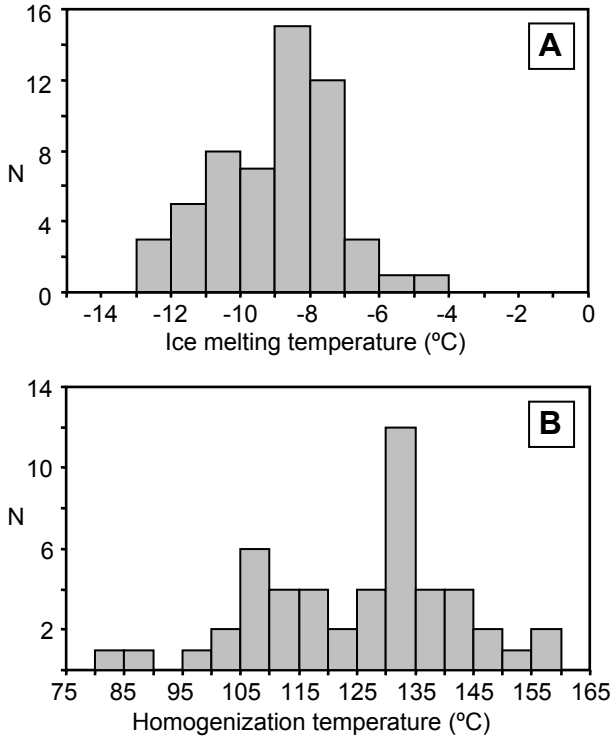
A
16
12
8
4
0
N
-14
-12
-10
-8
-6
-4
-2
0
Ice melting temperature (ºC)
B
14
10
6
2
N
75
85
95
105
115
125
135
145
155
165
Homogenization temperature (ºC)

Figure 6

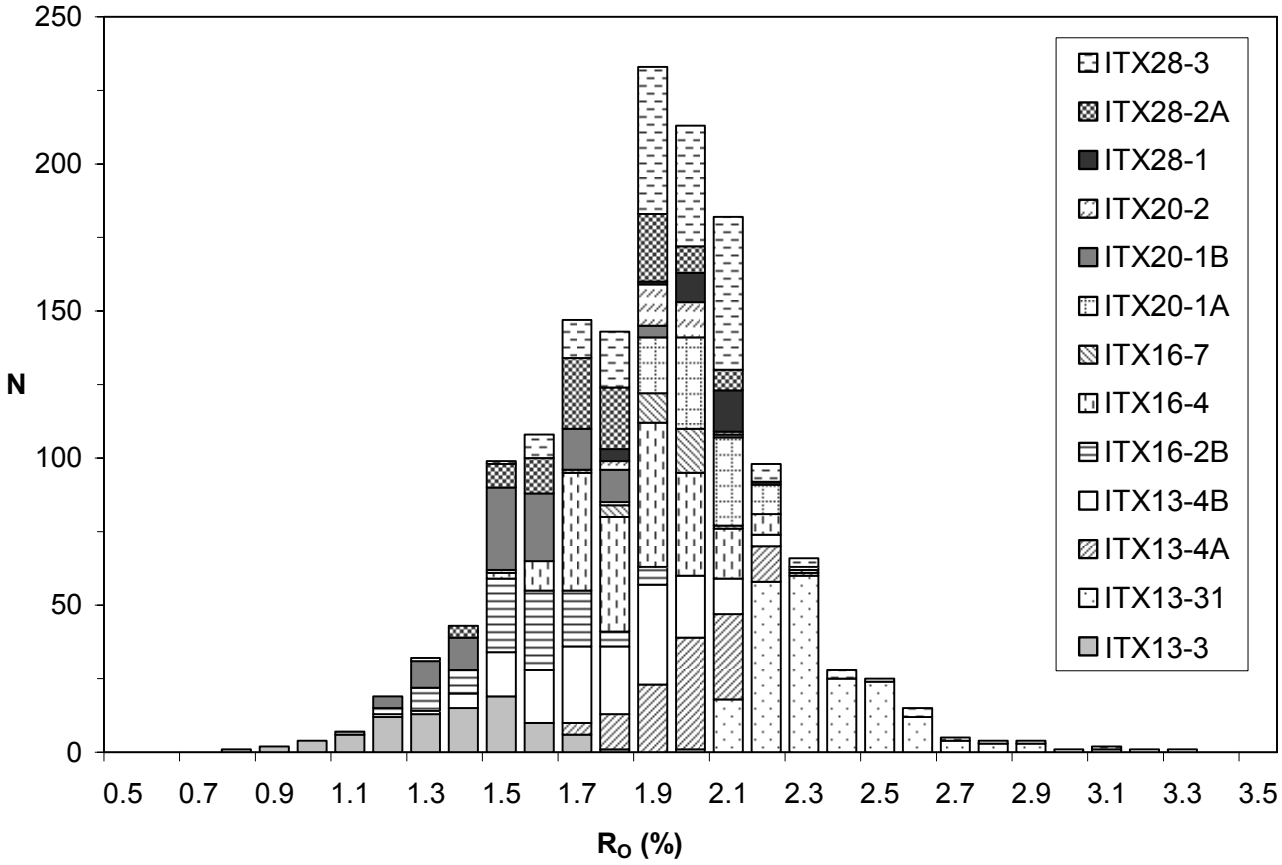
250
200
150
100
50
0
N
0.5
0.7
0.9
1.1
1.3
1.5
1.7
1.9
2.1
2.3
2.5
2.7
2.9
3.1
3.3
3.5
R_O (%)
ITX28-3
ITX28-2A
ITX28-1
ITX20-2
ITX20-1B
ITX20-1A
ITX16-7
ITX16-4
ITX16-2B
ITX13-4B
ITX13-4A
ITX13-31
ITX13-3

Figure 7

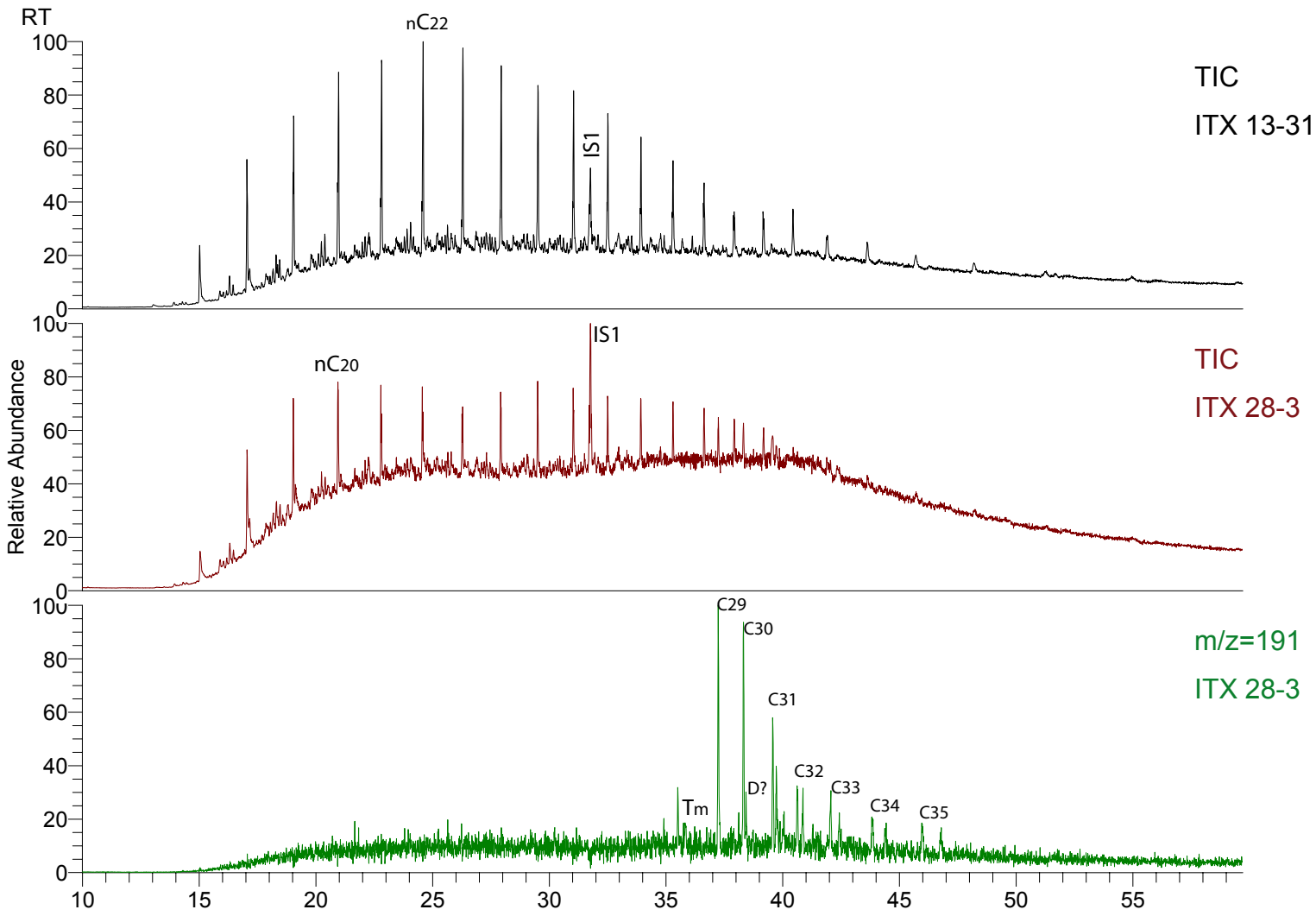
RT
nC22
IS1
TIC
ITX 13-31
Relative Abundance
nC20
IS1
TIC
ITX 28-3
C29
C30
C31
C32
C33
C34
C35
Tm
D?
m/z=191
ITX 28-3
10
15
20
25
30
35
40
45
50
55

Figure 8

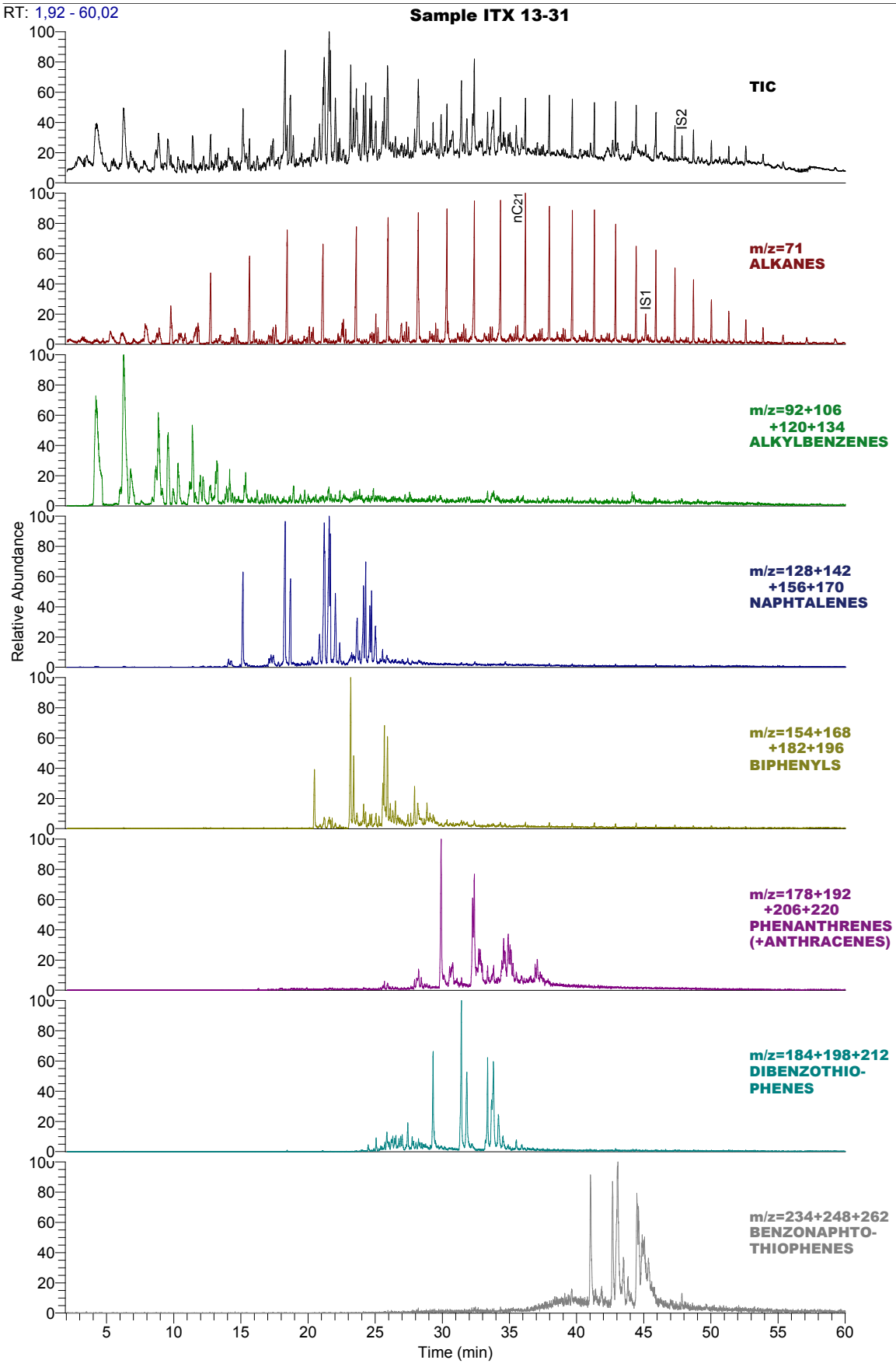
RT: 1,92 - 60,02
Sample ITX 13-31
TIC
IS2
nC21
IS1
m/z=71
ALKANES
m/z=92+106
+120+134
ALKYLBENZENES
m/z=128+142
+156+170
NAPHTALENES
m/z=154+168
+182+196
BIPHENYLS
m/z=178+192
+206+220
PHENANTHRENES
(+ANTHRACENES)
m/z=184+198+212
DIBENZOTHIO-
PHENES
m/z=234+248+262
BENZONAPHTO-
THIOPHENES
Relative Abundance
Time (min)

Figure 9

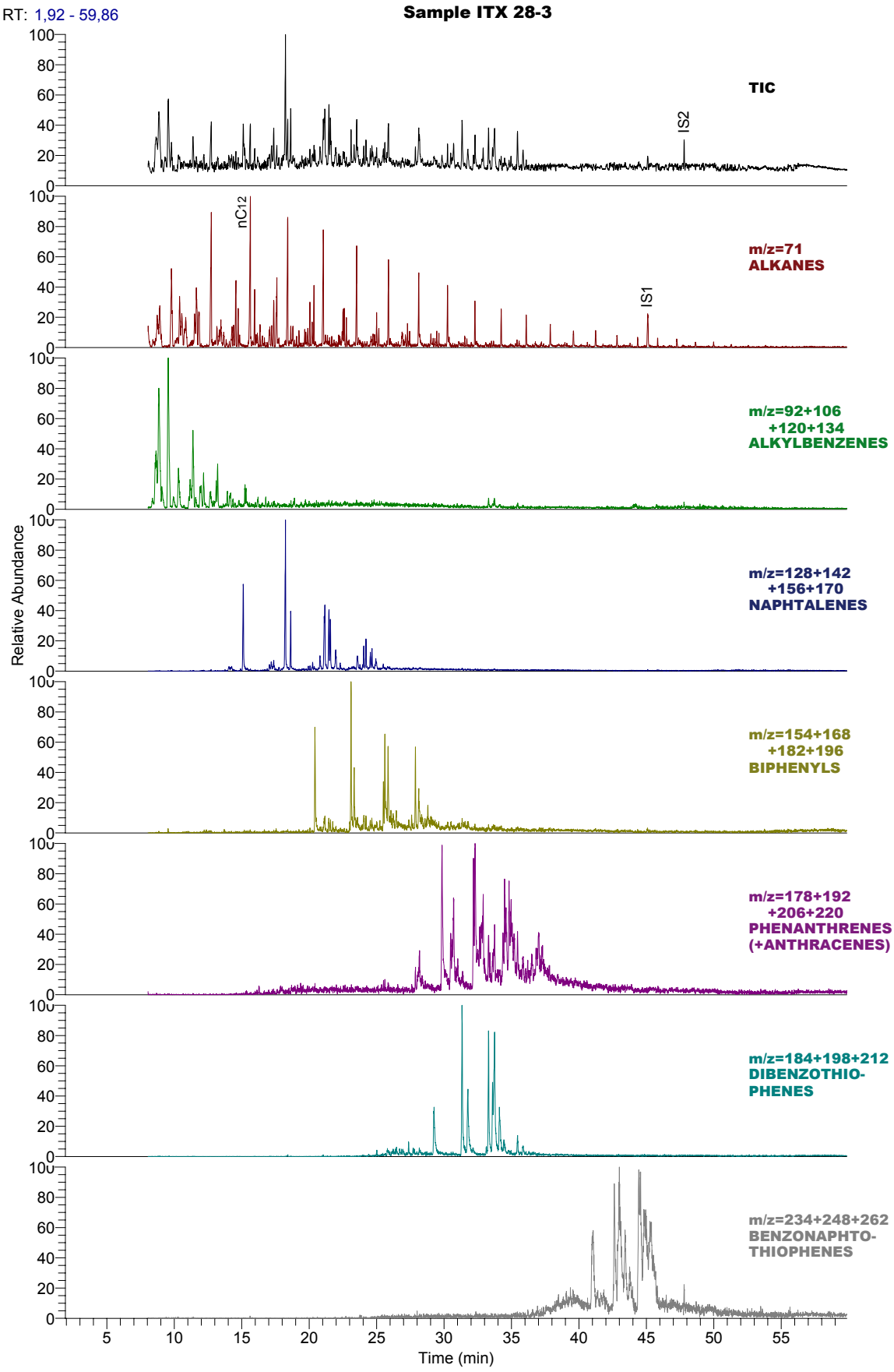
RT: 1,92 - 59,86
Sample ITX 28-3
TIC
IS2
nC12
m/z=71
ALKANES
IS1
m/z=92+106
+120+134
ALKYLBENZENES
m/z=128+142
+156+170
NAPHTALENES
m/z=154+168
+182+196
BIPHENYLS
m/z=178+192
+206+220
PHENANTHRENES
(+ANTHRACENES)
m/z=184+198+212
DIBENZOTHIO-
PHENES
m/z=234+248+262
BENZONAPHTO-
THIOPHENES
Relative Abundance
Time (min)

Figure 10